Epipolar rectification of a generic camera

Marc Pierrot Deseilligny, Ewelina Rupnik

Epipolar rectification of a generic camera

Marc Pierrot Deseilligny[1*] and Ewelina Rupnik[1]

[1*]LASTIG, Univ Gustave Eiffel, ENSG, IGN, Saint-Mande, F-94160, France.

*Corresponding author(s). E-mail(s): marc.pierrot-deseilligny@ensg.eu;
Contributing authors: ewelina.rupnik@ign.fr;

Abstract

We propose a generic method for epipolar resampling that is not tied to a specific camera model. We demonstrate the effectiveness of the approach on a central perspective, pushbroom and pushbroom panoramic camera models. We also devise an *epipolarability index* that measures the suitability of an image pair for epipolar rectification, and provide a formal derivation of the ambiguity bound to epipolar resampling.

Keywords: epipolar rectification, generic camera, pushbroom sensor, central perspective

1 Introduction

The epipolar geometry of images plays a central role in many applications in the field of photogrammetry and computer vision. In the stereo-reconstruction pipeline, it is used twice:

1. In the camera pose orientation step, when computing the relative orientation of a pair of images from their corresponding points. Assuming the projection follows the central perspective and the internal calibration is known, one can compute the epipolar geometry of the images using the essential matrix. Finally, the relative orientation is recovered (3).
2. In the image dense matching step, where the epipolar rectification simplifies the correspondence search because for any point (x_1, y) in image I_1,

its correspondence is some point (x_2, y) in image I_2. Therefore, finding correspondences across images is reduced to a 1-dimensional problem (1D).

In this paper, we only look at the epipolar rectification problem and more specifically its application to a generic camera model.

1.1 Related works

Rectifying a central perspective camera stereo pair involves transforming their original epipolar geometry to a canonical form where: (a) their focal planes are coplanar, and (b) their conjugate epipolar lines are colinear, and parallel to the camera's x-axis. From the algebraic standpoint, this is equivalent to applying two 2-dimensional (2D) projective transformations to both images of the stereo pair. Several approaches to computing such transformations have been proposed over the course of the last 30 years. For a calibrated stereo pair (i.e. with known camera projection matrices), there exists a unique rectifying transformation, up to a rotation along the baseline (3). In an uncalibrated case, the solution is obtained by factoring out two 2D homographies from the fundamental matrix.

Unlike the central projection camera model, pushbroom-like sensors acquire each image row from a different perspective center. As a consequence, the epipolar lines are neither straight lines, nor are they conjugate across the image (5). One way to overcome this particularity is to simplify the projection function with a 2D affine (10; 14) or a parallel projection model (8). Such approximations usually come at the price of precision, especially with the increasing camera field-of-view or in mountainous scenes. By extending the 2D affine model with two quaratic terms, Okamonoto *et al.* (1) demonstrates improved performance on SPOT images. In the context of dense image matching, de Francis *et al.* (2) improves the precision by partitioning the images into small patches, for which indepedent affine rectifictions are computed. Alternatively, and with equally good precision, Oh (9) uses the *Rational Polynomial Coefficients* (RPCs) to map the epipolar curves across the full size images with lines, in a piecewise approach, followed by a global rectification transformation using a polynomial function of 3^{rd} order.

1.2 Contributions

Our research work proposes an epipolar geometry rectification method that is not tied to any camera physical model. We provide a theoretical derivation and demonstrate the effectiveness of the approach on a range of models, including Pleiades images (pushbroom), the Corona images (panoramic pushbroom) and a consumer grade camera images (central perspective). The method resembles Oh's (9) approach in that it exploits the point correspondences to find the polynomial mapping to epipolar geometry. However, unlike the work of Oh (9), we do not require that the camera geometric model is known. We demonstrate that in some circumstances, point correspondences obtained from an image processing routine, e.g. SIFT (6), can serve to find the epipolar resampling.

Finally, we formally derive the ambiguity of the epipolar geometry, and propose an *epipolarability index* that quantitatively describes the existence of epipolar geometry between a pair of images.

In the remainder of this publication, we first outlay the mathematical background of the epipolar geometry, identify conditions required for its existence and establish its degree of ambiguity (Section 2). Then, we introduce our method (Section 3), and conclude with experiments on different datasets, with and without the geometric model (Section 4).

2 The mathematics of epipolar geometry in the generic case

2.1 Formalisation and notation of projections

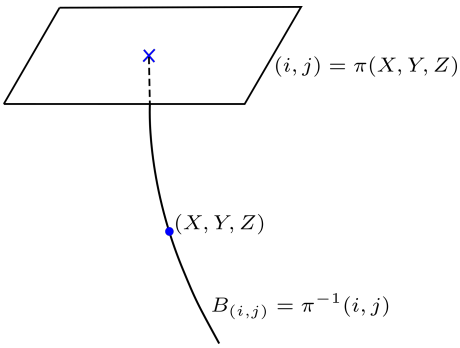

Fig. 1: A projection and a bundle.

We define the geometric sensor model of an image by a projection function π, that computes, for a given 3D point, its 2D projection in the image:

Definition 1 (Generic geometric sensor model) *Illustrated in Figure 1.*

A geometric sensor model π is a $\mathcal{C}^\infty$ mapping from ground space ($\mathbb{R}^3$) to image space ($\mathbb{R}^2$):

$$\pi : \mathbb{R}^3 \to \mathbb{R}^2, (X,Y,Z) \to (i,j) = \pi(X,Y,Z). \tag{1}$$

Next, we define the bundles of a projection:

Definition 2 (Bundle) For $p_k \in I_k$ we note $\mathcal{B}_k(p_k)$ the bundle corresponding to $\pi_k^{-1}(p_k)$. When there is no ambiguity, we note identically $\mathcal{B}_k(P)$, where $P \in \mathbb{R}^3$, the bundle corresponding to $\pi_k^{-1}(\pi_k(P)) = \mathcal{B}_k(\pi_k(P))$.

Later, for simplicity, we will use the quasi-vertical hypothesis, which allows us to extend π to a bijective mapping of $\mathbb{R}^3$ and compute its inverse.

Definition 3 (Quasi-vertical camera model) We say that the projection is quasi-vertical if the following mapping $\widetilde{\pi}$ is a diffeomophism of $\mathbb{R}^3$:

$$\widetilde{\pi} : \mathbb{R}^3 \to \mathbb{R}^3, (X, Y, Z) \to (i, j, Z) = \widetilde{\pi}(X, Y, Z), with (i, j) = \pi(X, Y, Z). \quad (2)$$

Given 2 images I_1 and I_2, the knowledge of their geometric models π_1 and π_2 reduces the matching between 2 images to a 1D problem. In fact, given a point p_1 in I_1, we can compute the 3D curve $\mathcal{B}_1(p_1)$ of ground points that project to p_1 in I_1, and compute its homologous curve in I_2 with $\pi_2(\mathcal{B}_1(p_1))$. We now define the H-compatible relation between two points by the following definition:

Definition 4 (H-Compatible, $\overleftrightarrow{\pi_1,\pi_2}$) *Illustrated in Figure 2.*

We say that p_1 in I_1 and p_2 in I_2 are $\pi_1 - \pi_2$ H-compatible, and write $p_1 \overleftrightarrow{\pi_1,\pi_2} p_2$, if the following condition is satisfied:

$$(\mathcal{B}_1(p_1) \cap \mathcal{B}_2(p_2) \neq \emptyset) \Leftrightarrow (\exists P \in \mathbb{R}^3 : \pi_1(P) = p_1, \pi_2(P) = p_2). \quad (3)$$

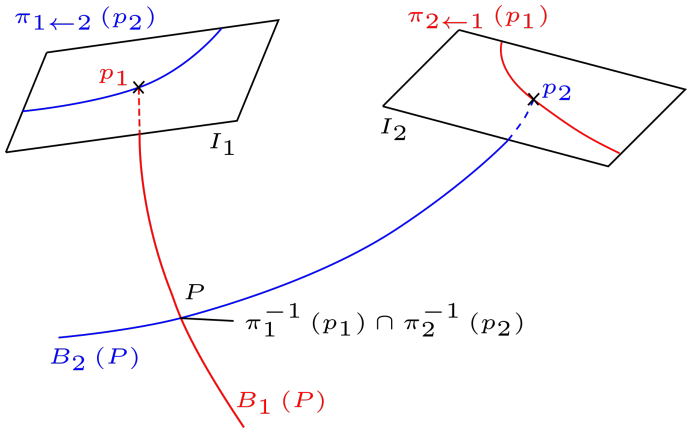

Fig. 2: Illustration of $\overleftrightarrow{\pi_1,\pi_2}$.

In image matching, the relationship $p_1 \overleftrightarrow{\pi_1,\pi_2} p_2$ means that p_1 and p_2 are potentially homologous.

2.2 Definition of the epipolar geometry

In fact, the previous relationships are sufficient to implement all the matching techniques and (π_1, π_2) can be used to define a matching process, taking

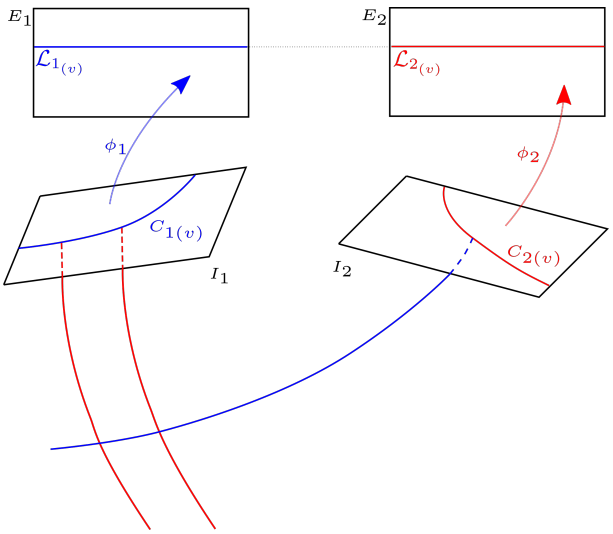

Fig. 3: Illustration of epipolar geometry.

advantage of the *a priori* knowledge of the scene geometry. That is, given a point in one image, we can easily follow its curve of potentially homologous points in the other image. This technique, which does not exploit the epipolar geometry, has the advantage of also being adaptable to multi-image matching. Epipolar geometry is therefore not strictly required for the image matching process.

The drawback of this approach is that it combines two different problems in the same procedure: the handling of the geometry and resampling and the matching process. When one is interested in the matching of a single image pair, the epipolar geometry can provide an elegant solution by separating the problem in two independent ones.

Definition 5 (Epipolar Geometry) *Illustrated in Figures 3 and 6.*

Let π_1, π_2 be two cameras and let ϕ_1, ϕ_2 be two diffeomorphisms of $\mathbb{R}^2$. We say that ϕ_1, ϕ_2 are an epipolar resamplings iff:

$$\forall e_1 = (u_1, v_1), e_2 = (u_2, v_2) : (v_1 = v_2) \Leftrightarrow (\phi_1^{-1}(e_1) \underset{\pi_1,\pi_2}{\Longleftrightarrow} \phi_2^{-1}(e_2)). \tag{4}$$

The matching of epipolar images is simplified because we know that the lines in two images are globally homologous.

Notation 1 (Epipolar line and curve.) We denote $\mathcal{L}_k(v)$ as the epipolar line of E_k defined by $v_k = v$. We also denote $\mathcal{C}_k(v)$ as the epipolar curve of I_k defined by $\mathcal{C}_k(v) = \phi_k^{-1}(\mathcal{L}_k(v))$

We can see that when epipolar geometry exists, the two curves $\mathcal{C}_1(v)$ and $\mathcal{C}_2(v)$ are globally homologous:

$$\mathcal{C}_1(v) = \pi_1(\pi_2^{-1}(C_2(v))); \; \mathcal{C}_2(v) = \pi_2(\pi_1^{-1}(C_1(v))). \tag{5}$$

2.3 Existence of the epipolar geometry

We now discuss the existence of the epipolar geometry. As it will be seen, the epipolar geometry generally does not exist, and when it does, it is not unique. We know that for any image pair following the central projection, there exists an epipolar geometry. However, with e.g. a cylindrical projection specific to many pushbroom satellites, the rigorous epipolar resampling is impossible (but close approximation generally exists).

We explain now why the epipolar geometry does not exist for any projections π_1, π_2 and is instead an exception. Let's define the surface $\mathcal{S}_v^k$ of $\mathbb{R}^3$ by:

$$\mathcal{S}_v^k = \pi_k^{-1}(\mathcal{C}_k(v)). \tag{6}$$

Following the definition of epipolar geometry above, it can be seen that $\mathcal{S}_v^1$ and $\mathcal{S}_v^2$ are the same surface $\mathcal{S}_v$:

$$\mathcal{S}_v^1 = \mathcal{S}_v^2 = \mathcal{S}_v. \tag{7}$$

In fact, for any $P \in \mathcal{S}_v^1$, set $e_1 = \phi_1(\pi_1(P)) = (u_1, v)$ and $e_2 = \phi_2(\pi_2(P)) = (u_2, v_2)$. We then have $\pi_1(P) \overleftrightarrow{\pi_1,\pi_2} \pi_2(P)$ because they are projections of the same point. Then, $v_2 = v$ according to Definition 5, and $P \in \mathcal{S}_v^2$. Furthermore, the $\mathcal{S}_v$ defines a foliation of $\mathbb{R}^3$, and it can be seen that:

$$\forall v \forall P \in \mathcal{S}_v : \mathcal{B}_1(P) \subset \mathcal{S}_v, \mathcal{B}_2 \subset \mathcal{S}_v, \tag{8}$$

which also leads directly from the definitions above because if $P \in \mathcal{S}_v$ then $\pi_k^{-1}(P) \in \mathcal{C}_k(v)$ (see Equation (6)), and $\pi_k^{-1}(\pi_k(P)) = \mathcal{B}_k(P) \subset \mathcal{S}_v$. However, in general, the existence of a stable foliation for the two bundle sets, as expressed in Equation (8), cannot be satisfied. We illustrate it in Figure 4. Furthermore, let π_1 and π_2 be again any two projections and suppose there exists a foliation satisfying the Equation (8). Then, let:

- P be any point in 3D space, and $\mathcal{S}_v$ be the surface such that $P \in \mathcal{S}_v$;
- $P_1 \neq P$ be a point on 3D curve $\mathcal{B}_1(P)$, $P_1 \in \mathcal{S}_v$, then $\mathcal{B}_2(P_1) \subset \mathcal{S}_v$;
- $P_2 \neq P$ be a point on 3D curve $\mathcal{B}_2(P)$, $P_2 \in S_v$, then $\mathcal{B}_1(P_2) \subset \mathcal{S}_v$.

As $\mathcal{B}_2(P_1)$ and $\mathcal{B}_1(P_1)$ are included in the same surface $\mathcal{S}_v$, they must intersect somewhere in a point Q. In the general case, the above statement is a contradiction because there is no reason that the condition $\mathcal{B}_2(P_1) \cap \mathcal{B}_1(P_2) \neq \emptyset$ is satisfied for any two sets of bundles (see Figure 4, right).

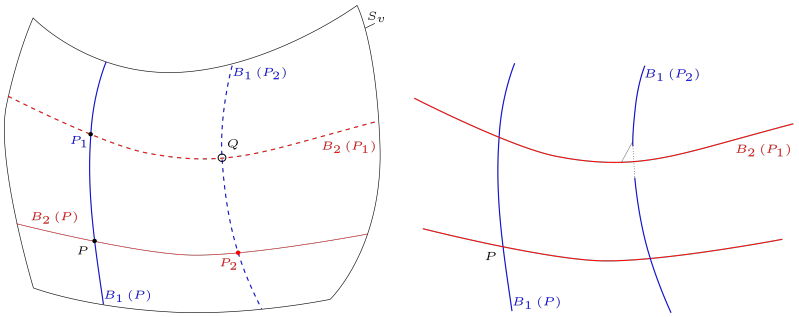

Fig. 4: Path closure. Left: in the epipolar case, the bundles are on the same level of the foliation and the intersection. Right: in the generic case, the paths don't intersect and no epipolar geometry exists.

2.4 A local characterization of the epipolar existence

In this section, we derive a local formula (i.e. a differential equation) that measures the existence of an epipolar geometry. We refer to it as the *epipolarability index*. This section is rather theoretical and can be omitted by readers mainly interested in practical applications.

Analogously to the proof in Section 2.3, we will make a computation of two-way paths, $\mathcal{B}_1$ then $\mathcal{B}_2$, as well as $\mathcal{B}_2$ then $\mathcal{B}_1$. Then, we express the Taylor expansion of the intersection distance between these two paths. For sake of simplicity, let's suppose that we are in a quasi-vertical acquisition geometry stated in definition 3[1], and in Figure 5, the point P is any point in $\mathbb{R}^3$. We then denote:

- the first path (P, P_1, Q_1) following $\mathcal{B}_1(P)$ then $\mathcal{B}_2(P_1)$, making a progression δ_1 on $\mathcal{B}_1(P)$ and δ_2 on $\mathcal{B}_2(P_1)$;
- a second path (P, P_2, Q_2) following $\mathcal{B}_2(P)$ then $\mathcal{B}_1(P_2)$, making a progression δ_2' on $\mathcal{B}_2(P)$ and δ_1' on $\mathcal{B}_1(P_2)$;
- $\overrightarrow{t_1(P)} = (x, y, 1)$ as the tangent to the bundle $\mathcal{B}_1$ in point P (and similarly $\overrightarrow{t_2}(P)$);
- and write $\frac{\partial F}{\partial z_1}$ to refer to the coordinate system $(i_1, j_1, z) = \widetilde{\pi}_1^{-1}(x, y, z)$, idem for $\frac{\partial F}{\partial z_2}$, and obviously as they are two different coordinate systems, we have in general $\frac{\partial F}{\partial z_1} \neq \frac{\partial F}{\partial z_2}$.

Now, for any pair of "small" values (δ_1, δ_2), we compute (δ_1', δ_2') which minimize the distance $|Q_1, Q_2|$ and express the canceling of the second degree Taylor expansion of this distance (the first degree can always be canceled out as we will see). Noting δ the max of all δ, the second degree Taylor expansion gives :

[1]Note that we could use curvilinear abscissa when this assumption is not be satisfied.

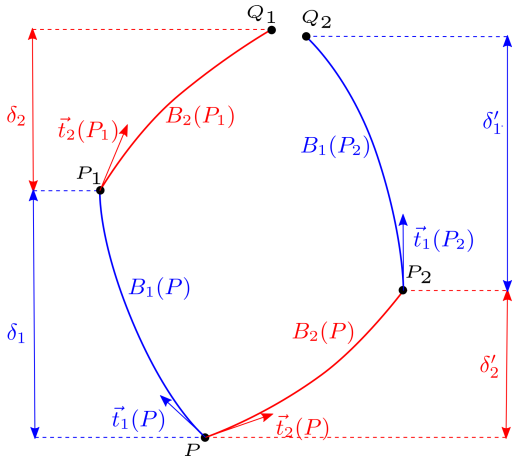

Fig. 5: Notation for local characterization of the epipolar existence.

$$P_1 = P + \delta_1 \overrightarrow{t_1(P)} + \frac{{\delta_1}^2}{2} \frac{\partial \overrightarrow{t_1}}{\partial z_1}(P) + \mathcal{O}(\delta^3) \tag{9}$$

$$Q_1 = P_1 + \delta_2 \overrightarrow{t_2(P_1)} + \frac{{\delta_2}^2}{2} \frac{\partial \overrightarrow{t_2}}{\partial z_2}(P_1) + \mathcal{O}(\delta^3) \tag{10}$$

$$\overrightarrow{t_2(P_1)} = \overrightarrow{t_2(P)} + \delta_1 \frac{\partial \overrightarrow{t_2}}{\partial z_1}(P) + \mathcal{O}(\delta^2) \tag{11}$$

Putting together Equations (9), (10), (11) we can perform a Taylor expansion of the path P to Q_1:

$$Q_1 = P + \delta_1 \overrightarrow{t_1(P)} + \delta_2 \overrightarrow{t_2(P)} + \frac{{\delta_1}^2}{2} \frac{\partial \overrightarrow{t_1}}{\partial z_1}(P) + \frac{{\delta_2}^2}{2} \frac{\partial \overrightarrow{t_2}}{\partial z_2}(P) + \delta_1 \delta_2 \frac{\partial \overrightarrow{t_2}}{\partial z_1}(P) + \mathcal{O}(\delta^3) \tag{12}$$

And similarly for P to Q_2 :

$$Q_2 = P + \delta'_2 \overrightarrow{t_2(P)} + \delta'_1 \overrightarrow{t_1(P)} + \frac{{\delta'_2}^2}{2} \frac{\partial \overrightarrow{t_2}}{\partial z_2}(P) + \frac{{\delta'_1}^2}{2} \frac{\partial \overrightarrow{t_1}}{\partial z_1}(P) + \delta'_1 \delta'_2 \frac{\partial \overrightarrow{t_1}}{\partial z_2}(P) + \mathcal{O}(\delta^3) \tag{13}$$

The first degree Taylor expansion of $Q_2 - Q_1$ gives :

$$Q_2 - Q_1 = (\delta'_1 - \delta_1) \overrightarrow{t_1(P)} + (\delta'_2 - \delta_2) \overrightarrow{t_2(P)} + \mathcal{O}(\delta^2) \tag{14}$$

To minimize $|Q_2 - Q_1|$, the first step is to cancel the first degree terms of $Q_2 - Q_1$. We assume that $\overrightarrow{t_2(P)}$ and $\overrightarrow{t_1(P)}$ are independant vectors[2] and we must then make $\delta'_2 - \delta_2$ and $\delta'_1 - \delta_1$ second degree terms:

[2] Otherwise, it would be a degenerate case for stereovision

$$\Delta_1 = \delta'_1 - \delta_1 = \mathcal{O}(\delta^2)\ ;\ \ \Delta_2 = \delta'_2 - \delta_2 = \mathcal{O}(\delta^2) \tag{15}$$

To develop $Q_2 - Q_1$ we can use the following identities that are direct consequences of Equation (15):

$$\delta_1\delta_2 - \delta'_1\delta'_2 = \mathcal{O}(\delta^3)\ ;\ \ {\delta_1}^2 - {\delta'_1}^2 = \mathcal{O}(\delta^3)\ ;\ \ {\delta_2}^2 - {\delta'_2}^2 = \mathcal{O}(\delta^3) \tag{16}$$

Subtracting Equation (12) from Equation (13), and using Equation (16), we can write :

$$Q_2 - Q_1 = \Delta_1\overrightarrow{t_1(P)} + \Delta_2\overrightarrow{t_2(P)} + \delta_1\delta_2\left(\frac{\partial\overrightarrow{t_2}}{\partial z_1}(P) - \frac{\partial\overrightarrow{t_1}}{\partial z_2}(P)\right) + \mathcal{O}(\delta^3) \tag{17}$$

We now translate the intersection of paths by canceling the second degree Taylor expansion in $Q_2 - Q_1$. We have three vectors, and their weighted sum can be null iff they are colinear.

Theorem 1 (Existence of epipolar geometry) *The epipolar geometry exists iff the following determinant is null:*

$$\left[\ \overrightarrow{t_1}\ \middle|\ \overrightarrow{t_2}\ \middle|\ \frac{\partial\overrightarrow{t_2}}{\partial z_1} - \frac{\partial\overrightarrow{t_1}}{\partial z_2}\ \right] = 0 \tag{18}$$

Remark 1 (Epipolar equation with central perspective camera) As an illustration on an easy case, we can see that this condition is trivially satisfied for a pair of central perspective cameras as we have the canceling of both terms as shown in Equation (19). This is because for a given point P, and any point P_1 on $\mathcal{B}_1(P)$, $\overrightarrow{t_2(P_1)}$ belongs to the epipolar plane $\mathcal{P}$. We have $\overrightarrow{t_2(P_1)} \in \mathcal{P}$, so $\frac{\partial\overrightarrow{t_2}}{\partial z_1} \in \mathcal{P}$, and as we have also $\overrightarrow{t_1(P)} \in \mathcal{P}, \overrightarrow{t_2(P)} \in \mathcal{P}$, the collinearity between $\overrightarrow{t_1(P)}$, $\overrightarrow{t_2(P)}$ and $\frac{\partial\overrightarrow{t_2}}{\partial z_1}(P)$ is thus proven:

$$\left[\ \overrightarrow{t_1}\ \middle|\ \overrightarrow{t_2}\ \middle|\ \frac{\partial\overrightarrow{t_2}}{\partial z_1}\ \right] = \left[\ \overrightarrow{t_1}\ \middle|\ \overrightarrow{t_2}\ \middle|\ \frac{\partial\overrightarrow{t_1}}{\partial z_2}\ \right] = 0 \tag{19}$$

2.5 Ambiguity of the epipolar geometry

When the epipolar geometry exists, the epipolar resampling is not unique. To demonstrate that our rectification method handles this ambiguity rigorously, we first describe it formally.

Let ϕ_1, ϕ_2 and ϕ'_1, ϕ'_2 be two epipolar resamplings. Following the depiction in Figure 6, for any v, consider the pair of lines $\mathcal{L}_1(v), \mathcal{L}_2(v)$ for which:

- $\phi_k^{-1}(\mathcal{L}_k(v))$ is the curve $\mathcal{C}_k(v)$ by definition of epipolar resampling;
- and $\phi'_k(\mathcal{C}_k(v)) = \phi'_k(\phi_k^{-1}(\mathcal{L}_k(v))$ is a line, also by definition of epipolar resampling;

- and in analogy, $\phi_1'(\phi_1^{-1}(\mathcal{L}_1(v))) = \phi_2'(\phi_2^{-1}(\mathcal{L}_2(v)))$.

Consequently we have the following constraints between two pairs of epipolar ressampling:

- $\phi_1'\phi_1^{-1}$ and $\phi_2'\phi_2^{-1}$ are diffeomorphisms transforming lines into lines;
- $\phi_1'\phi_1^{-1}$ and $\phi_2'\phi_2^{-1}$ define the same global transformation on lines (i.e. if $\phi_1'(\phi_1^{-1}(\mathcal{L}_1(v))) = \phi_2'(i\phi_2^{-1}(\mathcal{L}_2(v)))$).

Vice versa, let ϕ_1, ϕ_2 be an epipolar resampling and let Λ_1, Λ_2 be diffeomorphisms that are stable for lines and make globally the same transformation on lines. We can thus note that $\Lambda_1 \circ \phi_1$ and $\Lambda_2 \circ \phi_2$ are also an epipolar resampling (see Figure 6).

Having devised the exact ambiguity, we can now define two constraints to impose on a unique epipolar resampling:

1. **Constraint on the uniqueness of the deformation** inside each line . For instance, one can impose that the colums remain constant (i.e. the deformation is only made on y), as given in Equations (20) and (21);
2. **Constraint on the global deformation** of lines[3]. For instance, by fixing the transformation of one image, as given in Equation (6).

Theorem 2 (Unique epipolar constraint) *If the epipolar geometry exists, there exists a unique epipolar resampling ϕ_1, ϕ_2 satisfying the following three constraints:*

$$\phi_1(x, y) = (x, y') \tag{20}$$
$$\phi_2(x, y) = (x, y') \tag{21}$$
$$\phi_1(0, y) = (0, y) \tag{22}$$

3 Proposed method for epipolar geometry resampling

3.1 Hypothesis and layout

3.1.1 Principles

The principle of the method is to use *H-Compatible* points p_1, p_2 to calculate a pair of functions ϕ_1, ϕ_2 that comply with the epipolar constraint, i.e. *"$\phi_1(p_1)$ and $\phi_2(p_2)$ are on the same line"*. As these epipolar functions are not unique, we parameterize the ϕ_k in Theorem 2, accordingly:

$$\phi_k(i, j) = (i, V_k(i, j)); \quad V_k : \mathbb{R}^2 \to \mathbb{R} \tag{23}$$

[3] i.e. where each line is transformed globally to another line

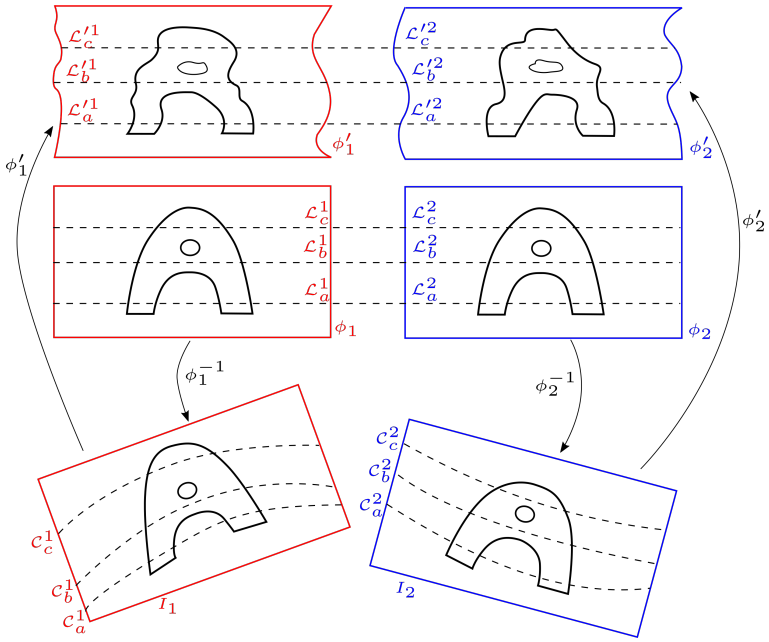

Fig. 6: Ambiguity of the epipolar geometry: two possible epipolar resamplings for a single stereo pair.

This parametrization implements the constraints of Equations (20) and (21). We will account for the constraint of Equation (22) in Section 3.2.1. To compute V_1, V_2, for any pair of *H-Compatible* points, we add an observation that constrains V_1 and V_2:

$$V_1(p_1) = V_2(p_2). \tag{24}$$

3.1.2 Hypothesis

The method takes two camera models π_1 and π_2 as inputs. These models are considered black-boxes that satisfy Equation (1), and for which no specific assumption is made on the physical model of the camera. In our `C++` implementation, the cameras are considered to be pure virtual classes offering the interface to Equation (1). In this paper, the examples processed by our method are pushbroom satellite models known by their RPCs and the central perspective. However, the only restriction imposed on the generic nature of the model is that the projection function is "smooth", i.e.:

- π are $\mathcal{C}^\infty$ functions, and
- the directions of epipolar curves vary within a limited range (for example, less than $\frac{\pi}{2}$).

Figure 7 illustrates the latter constraint. The left image presents a set of epipolar lines with too large direction variations. The right images represent pairs of epipolar lines whose directions change within a small range, therefore suitable for the proposed resampling method.

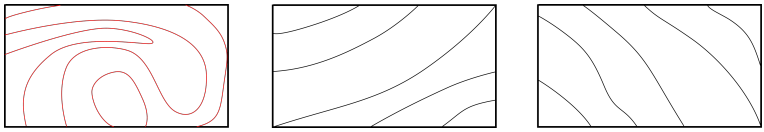

Fig. 7: Epipolar lines. Left: not handled by our method; Right: acceptable by our method.

3.1.3 Estimation of the center and the global direction

Before calculating the rectifying functions V_k, we need to compute a coordinate system where epipolar lines are globaly horizontal. This requirement is a consequence of equation (23), and is illustrated by Figure 8:

- The left image of Figure 8 presents a case where epipolar curve are quasi-vertical and for which an epipolar correction of Equation (23), without an initial rotation, is impossible;
- The center image of Figure 8 presents a case where epipolar curve are slanted; In this case epipolar correction according to equation (23) is possible but leads to important distorsion in the image, as can be seen in the image on the right.

Therefore, for each image we estimate the average direction $\vec{D}_k$ of their epipolar lines, and a rotation R_k is applied on the input set of points p:

$$R_k(p) = \frac{p - C_k}{\vec{D}_k}, \tag{25}$$

where C_k is the centroid of the set of points. The epipolar lines are now globally horizontal and the subsequent epipolar deformation is computed on the rotated data points.

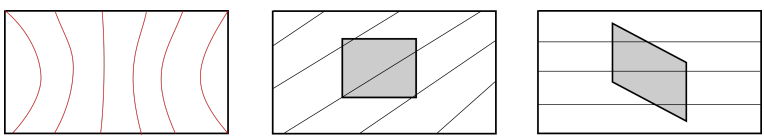

Fig. 8: Left: Quasi-vertical epipolar curve for which correction with Equation (23) is impossible. Middle and right: slanted curves for which epipolar rectification with Equation (23) is possible but generates significant distortion.

3.1.4 Layout

The layout of the method follows three steps: (1) estimate the global direction of epipolar lines; (2) estimate F_1, F_2 as the local epipolar rectification in the coordinate system linked to the global direction; (3) estimate the final epipolar rectification as a composition of F_1, F_2 and the rotation. A more formalized description of the algorithm is given in Algorithm 1.

Algorithm 1 Epipolar(π_1,π_2). *Layout of the algorithm for computing the epipolar rectification from camera models*

Use π_1, π_2 to estimate a set of *H-Compatible* points $\mathcal{H} = \{(p_1, p_2)\}$:
Estimate centers C_1 and C_2;
Estimate global direction of epipolars $\vec{D}_1$ and $\vec{D}_2$,
Estimate rotations R_1, R_2 according to Equation (25)
for all $p_1, p_2 \in \mathcal{H}$ **do**
  set: $q_1 = R_1(p_1)$, $q_2 = R_2(p_2)$
  add equation: $V_1(q_1) = V_2(q_2)$
end for
estimate with the least squares method V_1 and V_2
set $F_k(x, y) = (x, V_k(x, y))$
set $\phi_k = F_k \circ R_k$ **return** (ϕ_1, ϕ_2)

3.1.5 Why does our method work?

Intuitively, it may not be obvious that the system of equations in Equation (24) is well posed. In fact, if there was a functional relationship between p_1 and p_2, as $p_1 = F(p_2)$, an infinity of solutions for (V_1, V_2) would exist, because for any function $V : \mathbb{R}^2 \to \mathbb{R}$ we can generate a solution $(V, V \circ F)$.

However, note that due to the 3D aspect of p_1 and p_2, there is *no* functional relationship between them which conduct to a more constrained system of equations. Instead of a functional relationship, we can generate "one to many" (and "many to one") correspondences as illustrated in Figure 9. For example, for a given point p_1, following the curve $\pi_2(\mathcal{B}_1(p_1))$, we can generate several points on the bundle (potentially an infinity) which results in many correspondences. To illustrate, if we take p_2^k to be k homologous points of p_1, we then have the equation:

$$V_1(p_1) = V_2(p_2^1)\ ;\ \ V_1(p_1) = V_2(p_2^2)\ ;\ \ V_1(p_1) = V_2(p_2^3) \ldots, \tag{26}$$

which in fact enforces this constraint:

$$V_2(p_2^1) = V_2(p_2^2) = V_2(p_2^3) \ldots \tag{27}$$

If we now look at left image of Figure 9, we see that Equation (27) imposes the constraint that a "piece of curve" is horizontal. In Section 3.3.1, we will

see a more detailed analysis explaining how the method can work even with configurations different than those depicted in Figure 9.

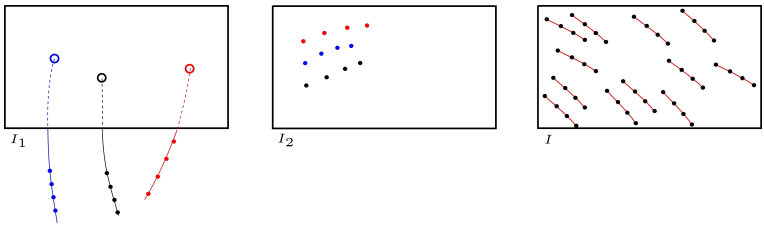

Fig. 9: Left: For each p_1, we generate several 3D points on $B_1(p_1)$. Middle: The multiple correspondences in I_2. Right: A dense network of curves in I_2.

3.2 Detailed implementation

3.2.1 Choice of a parametric functional space

We need to select a space of parametric functions to represent V_1, V_2. The only constraint is that V_1, V_2 are $\mathcal{C}^\infty$ functions, and that the additional constraint in Equation (22) is valid.

Classically, when parameterizing a set of functions $\mathcal{C}^\infty$, a "natural" candidate is the set of polynomials of a given degree. We know that the function will be $\mathcal{C}^\infty$ and, according to the Stone-Weierstrass theorem (15; 13) (which says that the space of polynomials is dense in the space of continuous functions), with a sufficiently high degree we will be able to accurately approximate any continuous function. A possible limitation of selecting high degree polynomial is over-fitting, which may lead to unwanted high frequency behavior. In our case, this problem should never arise as the measurements are synthesized from the projection functions π_1, π_2, which provides sufficient redundancy (for instance, hundreds of times more measurements than constraints). Note, however, that some precautions must be taken with respect to the polynomial degree when using our method with image correspondences, without the geometric model (see Section 3.3.1).

If d is the selected degree, the two vectors of unknowns $C^1_{a,b}, C^2_{a,b}$, corresponding to coefficients of the polynomials are:

$$V_k(p) = V_k(i,j) = \sum_{a=0}^{d} \sum_{b=0}^{d-a} C^k_{a,b} i^a j^b. \tag{28}$$

3.2.2 Imposing constraints on global lines deformation

When applying the constraint of equation (22) to equation (28), we have $i = 0$, hence we can suppress all terms i^a for $a \neq 0$. The constraint equation then reads:

$$V_1(0,j) = j = \sum_{b=0}^{N} C_{0,b}^1 j^b \tag{29}$$

In the equation above, j on the left and the sum on the right are both polynomials. If the two polynoms are equal on a interval, their coefficient must be equal . This constraint fixes the $C_{0,k}^1$: $C_{0,1}^1 = 1$ and $C_{0,k}^1 = 0$ otherwise. Using the Kronecker delta, we can write:

$$C_{0,k}^1 = \delta_{1,k} \tag{30}$$

3.2.3 Generation of points, computation of the direction and centers

The points from π_1 and π_2 are generated twice, using each image as the master. The bundles are always generated from the master images. The Algorithm 2 presents the generation of the points with I_1 as the master, as well as the computation of the global direction and the points' centers.

Algorithm 2 GenerateData(). *Compute a list $L_{1,2}$ of $\pi_1 - \pi_2$ H-compatible pairs with I_1 as the master image. Compute also the center C_1 of points in I_1 and the global direction $\vec{D}_2$ for epipolar curves of I_2.*

$L_{1,2} \leftarrow ()$; $C_1 \leftarrow (0,0)$; $\vec{D}_2 \leftarrow \overrightarrow{(0,0)}$; $N \leftarrow 0$
for $p_1.x = 0$ to X_1 **Step** $\delta_{x,y}$ **do**
  for $p_1.y = 0$ to Y_1 **Step** $\delta_{x,y}$ **do**
    for $z = Z_0$ to Z_1 **Step** δ_z **do**
      $p_2 = \pi_2(\widetilde{\pi}_1^{-1}(p_1, Z))$
      $p_2' = \pi_2(\widetilde{\pi}_1^{-1}(p_1, Z + \delta_z))$
      if $p_2 \in I_2 \ \wedge \ p_2' \in I_2$ **then**
        $L_{1,2}.append((p_1, p_2))$
        $C_1 \leftarrow C_1 + p_1$
        $\vec{D}_2 \leftarrow D_2 + \frac{\overrightarrow{p_2 p_2'}}{|p_2 p_2'|}$
        $N \leftarrow N + 1$
      end if
    end for
  end for
end for$C_1 \leftarrow \frac{C_1}{N}$; $\vec{D}_2 \leftarrow \frac{\vec{D}_2}{N}$

Once the centers C_1, C_2, directions $\vec{D}_1, \vec{D}_2$ and the list $L_{1,2}$ are computed, they are used to normalize the measurements and make the direction globally horizontal by applying Equation (25) to all elements of the list.

3.2.4 Estimating the rectification

As the measurements are synthetic and without outliers, we can directly solve the equations with the linear least squares method. Let's sum up all previous steps. Let d be the degree of the polynomials, and the unknowns are the coefficient of the polynomials V_1 and V_2. There are $\frac{(d+1)(d+2)}{2}$ unknowns for V_2 and $\frac{(d+1)(d+2)}{2} - (d+1)$ for V_1, taking into account the constraint in Equation (30). For each pair of normalized points q_1, q_2 (see Algorithm 1) we add the Equation (28) to the least squares equation system. We then estimate the V_1, V_2 and obtain:

$$\varphi_k(p) = \varphi_k(i,j) = (i, V_k(i,j)) \; ; \quad \phi_k = \varphi_k \circ R_k \tag{31}$$

Estimating the inverse function

The natural way to resample I_k in E_k (see Figure 2) is to write:

$$E_k(p) = I_k(\phi_k^{-1}(p)). \tag{32}$$

Therefore, to rectify an image, we also need to calculate the inverse function. The inverse of R_k is obvious. For computing the inverse of φ_k, we exploit the fact that if φ is invariant for the column, then φ^{-1} is invariant too. Consequently, we can parametrize it with a function $W : \mathbb{R}^2 \to \mathbb{R}$ as:

$$\varphi_k^{-1}(p) = \varphi_k^{-1}(u,v) = (u, W_k(u,v)) \tag{33}$$

To estimate W, we follow the same rationale as in Section 3.2.1, and use the base of a polynomial function. Once the V_k are known, we generate for each point $p_k = (i,j)$ in $L_{1,2}$ an observation:

$$W_k(i, V_k(i,j)) = j \tag{34}$$

If we want to ensure that the computed inverse is sufficiently close to the "real" inverse, we can increase the polynomial's degree (in our implementation, we typically use the degree of $d+4$). It has no side effects as long as we maintain high redundancy.

3.3 Epipolar resampling without the geometric model

3.3.1 Resampling with image correspondences only

"Is it possible to use the proposed method to compute the epipolar geometry if we have image point correspondences (i.e., image features) between the image pairs but we don't know their geometric models?" There is NO straightforward answer to whether it is possible or not. In general, it is not possible, but it becomes possible when the relief (i.e., the 3D scene) is not smooth and we constraint the resampling be more or less smooth.

The rationale behind trying to use exclusively image correspondences comes directly from Algorithm 1. As one can see, it does not matter if the point correspondences are extracted with the help of some geometric model (as with

Algorithm 2) or from an image processing method not requiring any *a priori* information on image geometry, e.g. SIFT (6). Hence, as long as we know the directions of the epipolar lines, our method is applicable.

However, when the point correspondences are computed with an image processing routine, there exists some functional relationship between them. Suppose that the 3D scene can be described by a function $Z = \mathcal{Z}(X, Y)$, and denote $S^{\mathcal{Z}}$ as the corresponding surface. For a point p_1 of I_1, denote $\widetilde{\pi}_1^{\mathcal{Z}}(p_1)$ as the intersection of $\mathcal{B}_1(p_1)$ and the surface $S^{\mathcal{Z}}$. Here, the function $\widetilde{\pi}_1^{\mathcal{Z}}$ is the inverse of the projection π_1 which relates the image I_1 and the surface $S^{\mathcal{Z}}$. We now see that there exists a functional relationship between all the point correspondences (p_1, p_2) and it follows this equation:

$$p_2 = (\pi_2 \circ \widetilde{\pi}_1^{\mathcal{Z}})(p_1) = F^{\mathcal{Z}}(p_1). \tag{35}$$

Therefore, as discussed in Section 3.1.5, in the most general case, it is impossible to recover the epipolar geometry from a set of correspondences.

This said, until now we have ignored what we said in Section 3.1.5, namely, that in the proposed method the functions V_1 and V_2 have to be "smooth". Let's reason again and suppose we have computed an epipolar geometry: $e_k = (u_k, v_k) = \phi_k(p_k) = (x_k, V_k(y_k)$ with $v_1 = v_2$ and V_k being a "smooth" function. We now want to analyse whether the geometry was ambiguous. We have

$$e_2 = (\phi_2 \circ \pi_2 \circ \widetilde{\pi}_1^{\mathcal{Z}} \circ \phi_1^{-1})(e_1) = P(e_1),$$

and so, we can write

$$(u_2, v_2) = P(u_1, v_1) = (u_1 + p_x(u_1, v_1), v_1),$$

where p_x is what is usually called the "parallax function". As in Section 3.1.5, for any function $W_2 : \mathbb{R}^2 \to \mathbb{R}$, let W_1 be the function defined by $W_1 = W_2 \circ P$. Then, for any (e_1, e_2), $(u_1, W_1(u_1, v_1))$ and $(u_2, W_2(u_2, v_2))$, we also satisfy the epipolar constraint as

$$W_1(u_1, v_1)) = W_2(P(u_1, v_1)) = W_2(u_2, v_2).$$

Is it possible that W_2 and $W_2 \circ P$ are both smooth functions? This depends on the smoothness of P. If P is itself a smooth function, then obviously for any smooth W_2, $W_2 \circ P$ will also be smooth and the epipolar resampling will be ambiguous. If we take the canonical example of a flat 3D scene, then $p_x = 0$, $P = Id$ and as $W_1 = W_2$, W_1 is smooth if W_2 is smooth. In this case the epipolar geometry is also ambiguous. However, if the scene has high frequency depth changes, then P also has high frequencies, and W_2 and $W_2 \circ P$ cannot both be smooth. This can be seen more formally by the following equation:

$$\frac{\partial W_2 \circ P}{\partial u} = \frac{\partial P}{\partial u} \frac{\partial W_2}{\partial u} \circ P. \tag{36}$$

As an example, for any point where the scene is not differentiable, we have $\frac{\partial P}{\partial u} = \infty$, and from the equation above, the term $\frac{\partial W_2}{\partial u} = 0$, because $W_2 \circ P$ is said to be smooth. With a polynomial W_2 of a limited degree and with a sufficient number of points, the term $\frac{\partial W_2}{\partial u} = 0$ leads to the realisation that W_2 depends only on v. Finally, including Equation (22), we have the polynomial $W_2 = Id$, which shows the uniqueness of the solution.

3.3.2 Estimating the directions without model

To use the resampling method with image features, we need a way to estimate the global directions of the epipolar lines, as it is done in Section 3.1.3 with the help of the geometric model. In the provided implementation we allow the user to provide the directions, or else the directions are computed automatically. For instance, in satellite along-track acquisitions, the user can easily deduce the directions, and it is certainly the "safer" option. The automated option is based in discretizing a number of directions in each image of a stereo pair, followed by a combinatorial exploration of all possible pairs of directions. For each direction pair, epipolar models (c.f., Section 3.2) with polynomials of degree 0 are computed. The residuals (i.e., the y-parallax) calculated on all image features serve as quality criterion in choosing the final global directions. Since the image features may contain outliers, residuals are evaluated using $L1$ norm .

Once the directions are known, the resampling polynomial is robustly calculated with a weighted iterative least-square approach as follows :

1. start with 1^{st} degree polynomial and evaluate it with $L1$ norms;
2. then, use the previous solution to weight the observations and evaluate 3^{rd} degree polynomial with the weighted least-squares method;
3. then, use the previous solution to weight the observations and evaluate 5^{th} degree polynomial with the weighted least-square method;
4. etc.

4 Experiments

We demonstrate the performance of the algorithm in two scenarios: with and without the geometric model of the camera. The results are evaluated in terms of the remaining *y-parallaxes*, and compared to competetitors: the method by Oh (9) for pushbroom geometries, and a resampling method implemented in MicMac for calibrated central perspective geometries (we refer to it as the *classical* method). The latter is equivalent of the epipolar resampling proposed by Fusiello (3) with the exception that it handles camera distortion parameters, hence, it does not require the undistorting of the images prior to the rectification. We evaluate our method against the central perspective geometry only for comparison purposes, because we dispose of ground truth epipolar geometries for this camera model. In practice, the classical method, which is founded on physical modeling with a minimal number of unknown, should be preferred.

To generate points correspondences in Algorithm 2, when the camera geometry is known, the points in the image space are defined as a grid of 100×100. The Z is the mean depth of the scene, and the step δ_Z is set such that 3 evenly distributed depths spaning the 3D space are obtained. Additionally, each image point is assigned a 4^{th}, random depth for evaluation. The min/-max depths representing the envelope of the 3D scene, can be inferred from the RPCs or from depths of the sparse structure (see Z_{buff} in Table 1).

Influence of different geometries of acquisition.

Five Pléiade-1A images with their corresponding RPC geolocations are first refined in a RPC-bundle adjustment (11). We then form pairs of images of varying base-to-height ratios ($^B/_H$) in the range $\in \langle 0.1, 0.45 \rangle$, and carry out epipolar resampling with *Ours* and Oh's methods. We also distinguish between *single orbit* and *multiple orbit* configurations. In Table 1 the maximum values of the remaining y-parallax are reported. The y-parallax is computed on a grid of image points generated with Algorithm 2. Note that these points are non-overlapping with the grid used for estimating the resampling polynomials. We can see that *Our* method outperforms the method by Oh in all instances and is insensitive to the acquisition geometry.

Comparison of resampling with and without the camera geometry.

To evaluate the performance of the proposed method on images without known camera geometry, we run epipolar resampling twice: with the camera model, and using SIFT features (6). In the latter scenario, the resampling polynomial was found across 6 iterations by progressively increasing the degree (the final polynomial being of 6^{th} degree). The comparison is done on a pair of Pléiade-1A images. In Figure 10 the per-pixel y-parallaxes are given. In all three scenarios the remaining parallax is of the same magnitude, $error_y < |0.05|$ pixel. The *Oh* and *Ours* method with the camera model give comparable results, while the approach with SIFT correspondences is clearly the best. The experiments with the camera model reveal a correlation between the remaining y-parallax and the 3D scene geometry. We believe this is due to unmodelled errors in RPC camera model. The approach based on SIFT correspondences uses points and is independent of the camera model hence no systematic error is present in the y-parallax map.

Epipolar resampling of panoramic pushbroom camera

Corona KH-4B images are analog images captured by the american reconnaissance satellites in the Cold War period (7). Since 1995 many Corona images are declassified and available to the public. Image processing and photogrammetry with Corona images remains difficult because the camera geometry is complex (12), and camera calibration certificates are rarely provided. In the absence of the known camera parameters, epipolar rectification with image features is an interesting alternative to allow for stereo-reconstruction. Figure 11 shows the image pair in its native geometry (i.e., panoramic pushbroom), the

SIFT features extracted on the full resolution images, as well as the epipolar curves. The resampling polynomial was found across 9 iterations by progressively increasing its degree (the final polynomial being of 9^{th} degree). As no ground truth is available, we evaluate the dataset visually in Figure 12 by providing a semi-global matching stereo-reconstruction and by drawing some epipolar lines. Because the images are subject to various distortions (i.e., panoramic, image scanning or image motion compensation distortions) as explained in (4), the remaining y-parallax in Figure 10(c) manifests systematic errors up to |0.5| pix. Such errors cannot be modelled with the chosen polynomial functions.

Epipolar resampling of central perspective camera

The experiments with the central perspective camera have a double objective. First we show that the proposed method works with pinhole cameras, and second we demonstrate the ambiguity of epipolar resampling when the scene can be represented by a smooth function, e.g., when it is flat (see Section 3.3.1). In Figure 13 the experiments are referred to as *Stairs* and *Floor*. The *Stairs* is an image pair of a staircase, so it is not flat. The *Floor*, as the name suggests, corresponds to the image pair of a floor, which is globally planar. We can observe that the epipolar resamplings computed with the camera models are comparable to the epipolar resampling with the *classical* method.

The experiment with the SIFT features is a confirmation of the theoretical analysis developped in 3.3 : with tie point only, it is possible to recover the epipolar geometry *if and only if* the relief contains high frequencies. Here method based on the SIFT features works well when the scene has a relief, and as expected fails on the planar scene (see the deformed epipolar image pair and the respective epipolar curves in Figure 13(c),(f)).

5 Discussion and perspective

We have presented of rigorous mathematical analysis of the epipolar resampling problem. In particular, we established the necessary and sufficient condition for the existence of an exact epipolar resampling and, when this condition is satisfied, established the degree of ambiguity of epipolar resampling. From this analysis we have derived a method for epipolar resampling of a generic pair of sensors that works as long a the existence criteria is approximately satisfied. The method computes the resampling functions by fitting analytical models which induce no deformation along the x-axis, and minimizes the y-parallax . We have demonstrated that the approach performs well on various camera geometries (central perspective, pushbroom, pushbroom panoramic). Experiments also showed suitability of the approach to resampling images with only image correspondences, when camera geometry is unknown. Note that the proposed method is not suitable for resampling images with large variations in the epipolar line directions. Future works include applying the method to multi-modal images, e.g. optical and radar.

Oh (9)				Ours			
B/H				B/H			
0.1	0.15	0.25	0.45	0.1	0.15	0.25	0.45
0.0055	0.0156	0.0144	0.0010	0.0036	0.0026	0.0026	0.0020

(a) Acquisitions from a **single orbit**.

Oh (9)				Ours			
B/H				B/H			
0.13	0.2	0.3	0.4	0.13	0.2	0.3	0.4
0.0381	0.0311	0.0343	0.0340	0.0101	0.0171	0.0143	0.0154

(b) Acquisitions from **multiple orbits**.

Table 1: Maximum value of the remaining y-parallax [pix]. Z_{buff} corresponds to half the depth of the volumne used in the resampling calculation and was set to 270m.

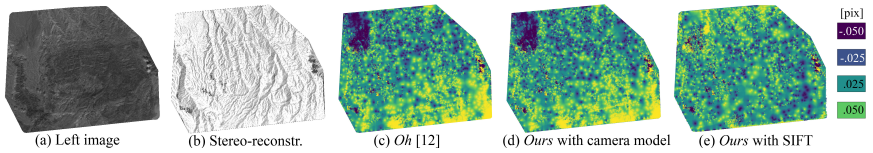

(a) Left image (b) Stereo-reconstr. (c) *Oh* [12] (d) *Ours* with camera model (e) *Ours* with SIFT

Fig. 10: Comparison of epipolar resampling with and without the camera geometry. (c)-(d) correspond to the per-pixel y-parallax computed with dense image matching in the direction perpendicular to the epipolar line.

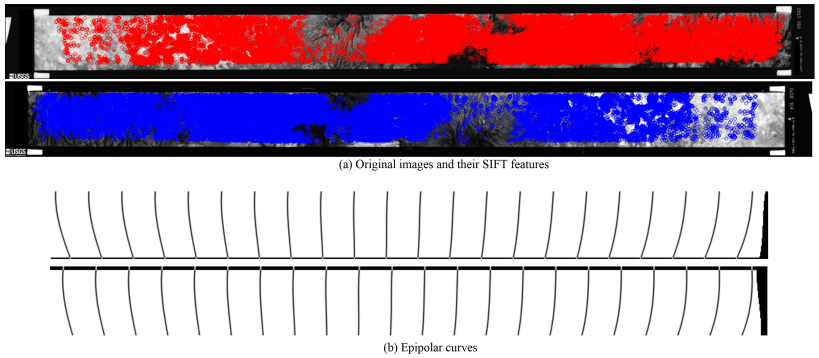

(a) Original images and their SIFT features

(b) Epipolar curves

Fig. 11: Corona KH-4B stereo pair.

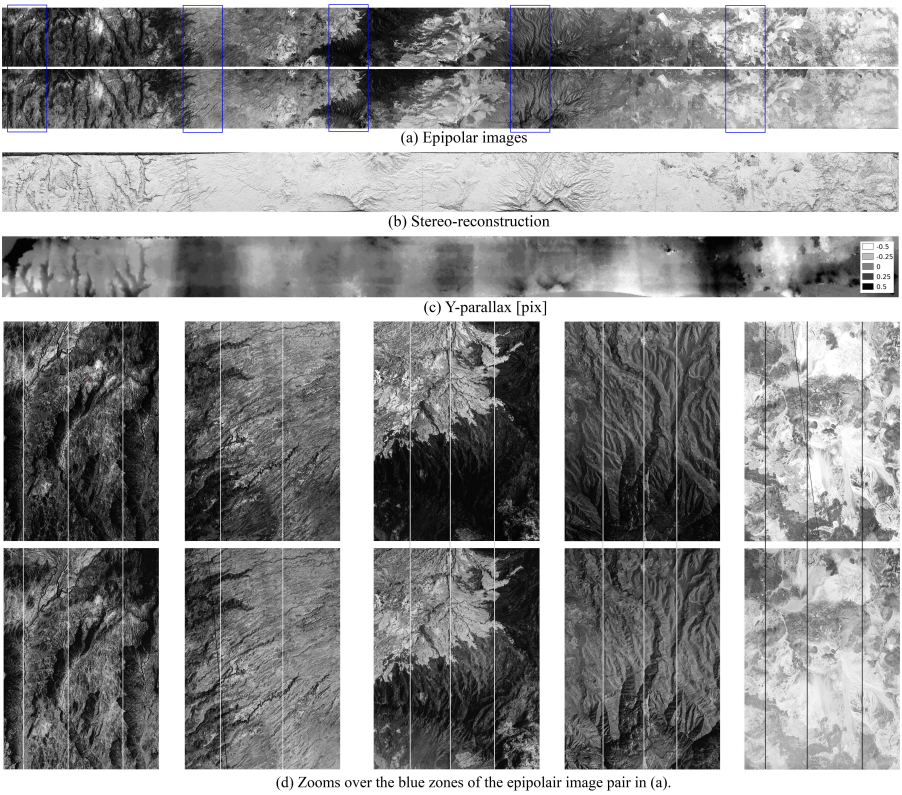

Fig. 12: Epipolar images generated from a Corona KH-4B stereo pair, its stereo-reconstruction and the remaining y-parallax. Epipolar lines are marked in white.

References

[1] Okamoto. A., T. Ono, S. Akamatsu, C. Fraser, S. Hattori, and Hasegawa H., *Geometric Characteristics of Alternative Triangulaion Models for Satellite Imagery*, in Proceedings of ASPRS 1999 Annual Conference, 1999.

[2] Carlo de Franchis, Enric Meinhardt-Llopis, Julien Michel, J-M Morel, and Gabriele Facciolo, *On stereo-rectification of pushbroom images*, in 2014 IEEE International Conference on Image Processing (ICIP), IEEE, 2014, pp. 5447–5451.

[3] Andrea Fusiello, Emanuele Trucco, and Alessandro Verri, *A compact algorithm for rectification of stereo pairs*, Machine vision and applications, 12 (2000), pp. 16–22.

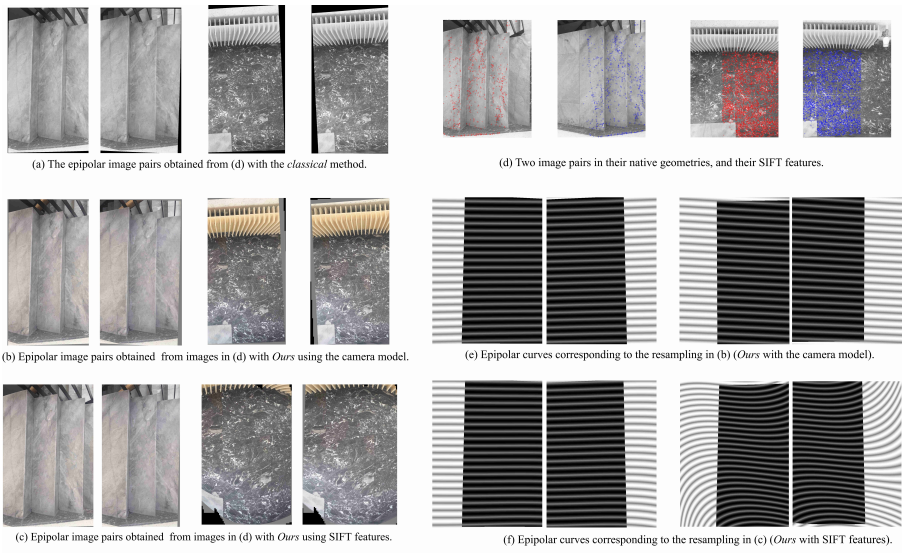

Fig. 13: Two experiments (*Staircase* and *Floor*) with the consumer grade camera. Epipolar pairs are obtained with three methods: the *classical* being equivalent of the resampling proposed by Fusiello (3) for calibrated cameras, *Ours* with the camera model, and *Ours* with the SIFT features. In (e) and (f) the black background corresponds to the overlapping zones in the image pairs.

[4] Wouter Gheyle, Jean Bourgeois, Rudi Goossens, and Karsten Jacobsen, *Scan problems in digital corona satellite images from usgs archives*, Photogrammetric Engineering & Remote Sensing, 77 (2011), pp. 1257–1264.

[5] Rajiv Gupta and Richard I Hartley, *Linear pushbroom cameras*, IEEE Transactions on pattern analysis and machine intelligence, 19 (1997), pp. 963–975.

[6] David G Lowe, *Distinctive image features from scale-invariant keypoints*, International Journal of Computer Vision, 60 (2004), pp. 91–110.

[7] FJ Madden, *The corona camera system: Itek's contribution to world stability, self-published*, (1996).

[8] Michel Morgan, Kyung-Ok Kim, Soo Jeong, and Ayman Habib, *Epipolar resampling of space-borne linear array scanner scenes using parallel projection*, Photogrammetric Engineering & Remote Sensing, 72 (2006), pp. 1255–1263.

[9] Jaehong Oh, *Novel Approach to Epipolar Resampling of HRSI and Satellite Stereo Imagery-based Georeferencing of Aerial Images*, PhD thesis,

The Ohio State University, 2011.

[10] Tetsu Ono, *Epipolar resampling of high resolution satellite imagery*, in Joint Workshop of ISPRS WG I/1, I/3 and IV/4 Sensors and Mapping from Space, Citeseer, 1999.

[11] E. Rupnik, M. Pierrot-Deseilligny, A. Delorme, and Y. Klinger, *Refined satellite image orientation in the free open-source photogrammetric tools Apero/MicMac*, ISPRS Ann. Photogramm. Remote Sens. Spatial Inf. Sci., (2016).

[12] Hong-Gyoo Sohn, Gi-Hong Kim, and Jae-Hong Yom, *Mathematical modelling of historical reconnaissance corona kh-4b imagery*, The Photogrammetric Record, 19 (2004), pp. 51–66.

[13] Marshall Harvey Stone, *Applications of the theory of boolean rings to general topology*, Transactions of the American Mathematical Society, 41 (1937), pp. 375–481.

[14] Mi Wang, Fen Hu, and Jonathan Li, *Epipolar resampling of linear pushbroom satellite imagery by a new epipolarity model*, ISPRS Journal of Photogrammetry and Remote Sensing, 66 (2011), pp. 347–355.

[15] Karl Weierstrass, *Über die analytische darstellbarkeit sogenannter willkürlicher functionen einer reellen veränderlichen*, Sitzungsberichte der Königlich Preußischen Akademie der Wissenschaften zu Berlin, 2 (1885), pp. 633–639.